

Modelling Dust Scattering in our Galaxy

Jayant Murthy,^{1*}

¹*Indian Institute of Astrophysics, Bangalore 560 034*

Accepted XXX. Received YYY; in original form ZZZ

ABSTRACT

I have used a Monte Carlo model for dust scattering in our Galaxy with multiple scattering to study the diffuse emission seen by the *GALEX* mission. I find that the emission at low and mid latitudes is fit well by scattering from dust grains with an albedo of 0.4 and $g = 0$ (isotropically scattering grains). However, only about 30% of the diffuse radiation at high Galactic latitudes is due to dust scattering. There is an additional component of $500 - 600 \text{ ph cm}^{-2} \text{ s}^{-1} \text{ sr}^{-1} \text{ \AA}^{-1}$ at all latitudes of an unknown origin.

Key words: surveys - ISM:general - dust, extinction - ultraviolet: general - ultraviolet: ISM

1 INTRODUCTION

The diffuse ultraviolet (UV) background was first detected by Hayakawa et al. (1969) but its faintness and the need for space-borne observations rendered progress slow for the next few decades (reviewed by Bowyer (1991) and Henry (1991) with a recent review by Murthy (2009)). There have been three large scale surveys of the diffuse ultraviolet sky over the last two decades. The first was the NUVEWS (The Narrowband Ultraviolet Imaging Experiment for Wide-Field Surveys) rocket flight (Schiminovich et al. 2001) which observed about 25% of the sky and noted the strong enhancement toward the Galactic plane with other bright spots near star forming regions such as Ophiuchus. More recently, the SPEAR/FIMS mission carried out a spectroscopic UV survey of the sky (Edelstein et al. 2006) and the Galaxy Evolution Explorer (*GALEX*) observed about 75% of the sky in two ultraviolet bands (Murthy 2014).

The diffuse background is generally thought to be due to starlight scattered by interstellar dust grains (Draine 2003) and models of the background have taken the incoming starlight and scattered it from the grains with different assumptions for the distribution of the exciting stars and the scattering dust (Jura 1979; Murthy & Henry 1995; Gordon et al. 2001; Schiminovich et al. 2001; Seon 2015). The availability of the all-sky *GALEX* data provides a powerful incentive to revisit the nature of the diffuse background as there have been suggestions that there are additional contributors which only reveal themselves in global studies (Hamden et al. 2013; Henry et al. 2015). I will describe here a new model

of the dust scattered background and its application to the *GALEX* observations in its two ultraviolet bands.

2 DATA

The *GALEX* spacecraft and its mission has been described by Martin et al. (2005) and Morrissey et al. (2007). The spacecraft was operational from 2003 June 7 until 2013 June 28 and observed most of the sky with a resolution of $5 - 10''$ in two UV bands. The FUV (1521 \AA) detector was plagued with intermittent failures of the high voltage power supply (HVPS) and finally ceased to work after 2009 May while the NUV (2361 \AA) instrument took data until the spacecraft was shut down. Most of the observations were made at high Galactic latitudes to avoid damage to the detectors from the bright diffuse background but there was a concerted effort to map brighter regions, including at low Galactic latitudes, near the end of the mission. Unfortunately, the FUV detector had already failed by this time so there are very few FUV observations at low latitudes.

Murthy (2014) used the *GALEX* data to construct maps of the diffuse background in both the FUV and NUV bands at 0.1° spatial resolution with the foreground emission (airglow and zodiacal light) subtracted (Fig. 1). The 1000 brightest stars are overplotted on the images as + signs with the size of the symbol proportional to the log of the brightness. There were no FUV observations in the Galactic plane because the detector failed in 2009 before observations of the brighter regions started. Gould's Belt is prominent in both bands as are halos around a number of bright stars (Murthy & Henry 2011). A full description of the methodology in the production of these maps is given in the paper and the maps

* E-mail: jmurthy@yahoo.com

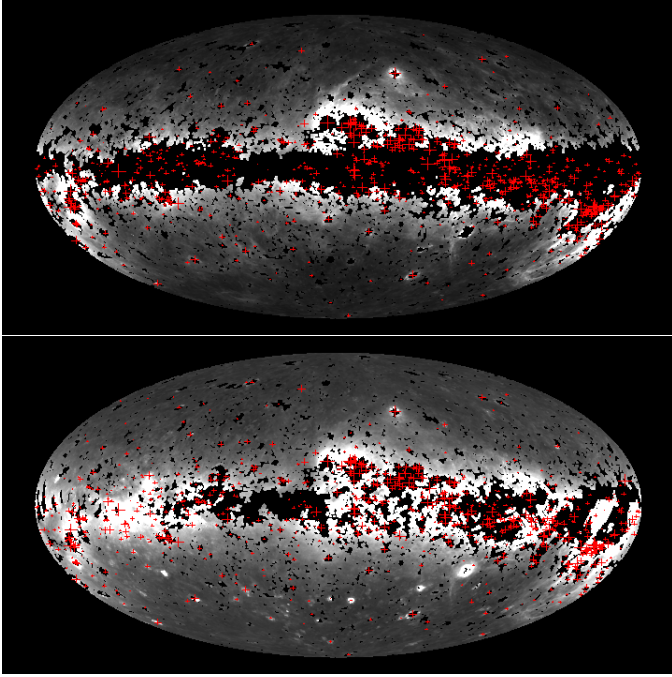


Figure 1. Observed fluxes in the FUV (top) and NUV (bottom) *GALEX* bands. The brightest stars are plotted as + symbols with the width of the symbol proportional to the log of the brightness at the respective wavelength. Black areas were not observed by *GALEX*.

are available from the High Level Science Products (HLSP) data repository¹ at the Space Telescope Science Institute.

3 MODELING

The radiative transfer problem in galaxies has been reviewed by [Steinacker et al. \(2013\)](#) with the much simpler problem of scattering only addressed in their Section 5.1. The problem can be broken into three parts: the stellar distribution; the dust distribution; and the scattering function. Photons are emitted by the stars and are scattered by the interstellar dust to the detector. The scattering function is invariably assumed to be the Henyey-Greenstein function ([Henyey & Greenstein 1941](#)) which is dependent on two free parameters: the albedo or reflectivity (a) and the phase function asymmetry factor ($g \equiv \langle \cos(\theta) \rangle$), where $g = 0$ implies that the grains scatter isotropically and $g = 1$ implies fully forward scattering grains. [Draine \(2003\)](#) has pointed out that the scattering may be more complex with a possible reverse scattering component but the data have not yet been good enough to support added complexity in the scattering function.

[Henry \(1977\)](#) showed that the interstellar radiation field in the UV could be calculated through an integration over the stars in a standard catalog. In this work, I have used the Hipparcos catalog ([Perryman et al. 1997](#)) which contains over 100,000 stars with the spectral type, B and V

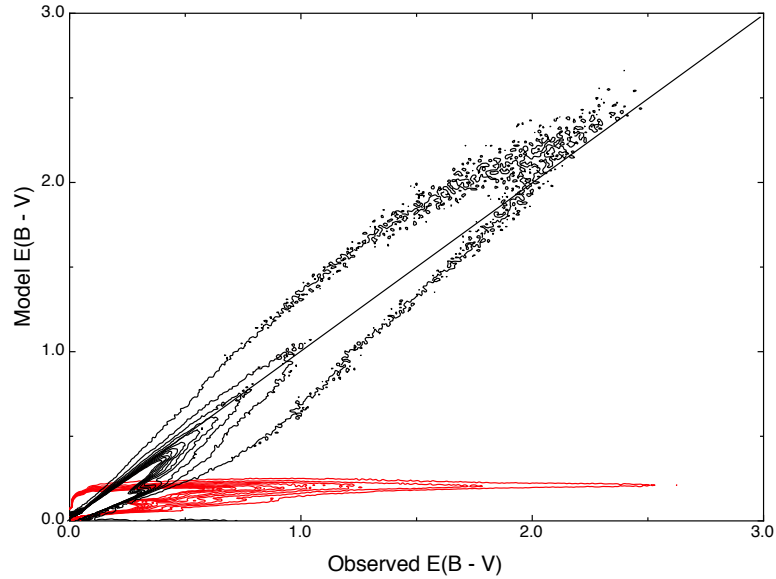


Figure 2. The correlation between the $E(B-V)$ from [Schlegel et al. \(1998\)](#) and the modelled $E(B-V)$ is shown as a density plot for Model 1 (red lines) and Model 2.

magnitude and distance of each star. I modelled the spectrum of each star using template spectra from [Castelli & Kurucz \(2004\)](#) with the translation from spectral type to model number as per their instructions². I then calculated the observed $E(B-V)$ from the cataloged B and V magnitudes and the intrinsic $(B-V)$ and finally the unreddened flux from each star assuming the Milky Way extinction curve of [Draine \(2003\)](#). This is the source function in my model: the number of photons from each star at the wavelength of interest.

I have tried two distributions in order to explore their effects on the scattered light. In the first, I have assumed that the gas density at the Galactic plane ($n[\text{H}]$) is 1 atom cm^{-3} , independent of longitude (Model 1) while I scaled the dust to match the observed $E(B-V)$ from [Schlegel et al. \(1998\)](#) in Model 2. In both cases, I assumed that there was a cavity of radius 80 pc around the Sun, corresponding to the Local Bubble ([Welsh et al. 2010](#)), and that the dust fell off from the Galactic plane with a scale height of 125 pc ([Marshall et al. 2006](#)). I have plotted the correlation between the observed and the modelled $E(B-V)$ for the two models in Fig. 2. My purpose in implementing these different models is to explore the factors affecting dust scattering rather than to accurately represent the distribution of interstellar dust.

A full radiative transfer model is complex because it is non-linear, non-local and multiwavelength in its formulation (reviewed by [Steinacker et al. 2013](#)). However, I am only concerned with the scattering of photons at single wavelengths which is a much simpler problem ([Steinacker et al. 2013](#), Section 5.1). I have written a set of routines in ANSI C which are available from the ASCL (bibcode: 2015ascl.soft12012M). The program is intended for use in the UV where the source distribution is well characterized and the volume of space is

¹ <https://archive.stsci.edu/prepds/uv-bkgd/>

² http://www.stsci.edu/hst/observatory/crds/castelli_kurucz_atlas.html

limited because of the high optical depth to UV radiation. However, it is modular and documented and may be freely modified for other purposes.

I will illustrate the program flow by following a single photon through its multiple scatterings. I generate a new random number from a uniform distribution in each step below except in Steps 2 and 5 where two numbers are needed to determine the direction of the photon. I have used the `genunf` (generate a random number from a uniform distribution) function from the `randlib` library³ to generate the random numbers and, if necessary, weighted the distribution to match the desired probabilities.

(i) A photon is emitted from a random star, weighted by the relative number of photons from that star, in a random direction. Each photon begins with a unit weight which will be reduced at each scattering.

(ii) Two random numbers are generated to calculate the direction of motion, one for θ (in the range from $0 - \pi$, measured from the z axis) and one for ϕ (in the range from $0 - 2\pi$). The position of the star is known in Cartesian coordinates (x, y, z) and the angles are converted into a direction vector assuming a step size of 1 bin.

(iii) Another random number is generated to determine the optical depth the photon travels. I have divided the Galaxy into $1000 \times 1000 \times 1000$ cells with a side of 1 pc and filled each cell with dust as per the individual model. The cross-section of the dust was taken from [Draine \(2003\)](#), which is a parametrization of the canonical extinction curve with $R (= A_V/E(B - V)) = 3.1$, the so-called Milky Way dust. I then follow the photon along until the cumulative optical depth along the path exceeds the predetermined value. This yields the Cartesian coordinates $x, y,$ and z of the scattering location.

(iv) I use the “effective peeling” technique ([Yusef-Zadeh et al. 1984](#)) to send a fraction of the photon back to the detector and subtract this (small) amount of energy from the effective weight of the photon. The detector in this case is assumed to observe the entire sky with an angular resolution of 0.1° per square bin.

(v) The effective weight of the photon is reduced by the albedo and a new scattering direction is determined as in step 2. The z direction is now the original direction of motion with the change of reference back to the original Cartesian coordinates using a rotation angle matrix.

(vi) The procedure is repeated from step 3 until the effective weight of the photon drops below a predetermined factor or the number of scatterings exceeds a specified limit ($n_{scatter}$). Note that single scattering corresponds to $n_{scatter} = 0$. In that case, the photon stops at the first interaction but the effective peeling method results in a flux at the detector.

4 RESULTS

I have plotted the total flux in the Galaxy at 1500 \AA as a function of the number of scatterings for different values of the optical constants along with the time taken for each

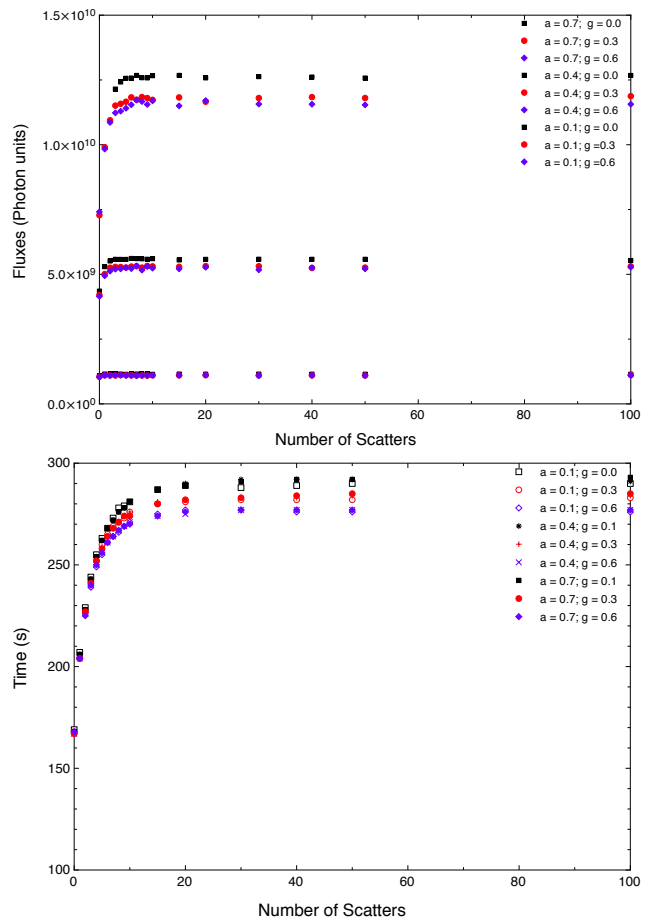


Figure 3. The total flux ($\text{ph cm}^{-2} \text{ s}^{-1} \text{ sr}^{-1} \text{ \AA}^{-1}$) in the simulation (left) is shown on the left and the amount of time per 10 million input photons (on a 3.7 GHz Quad-Core Intel Xeon E5 MacPro) is shown on the right. In both, the maximum number of scatterings per input photon before terminating the run is shown on the x axis. Each point represents a run of 10 million input photons with different value of a and g .

run in Fig. 3. The flux saturates at about 5 scatterings per photon and I have therefore capped the number of scatterers at that level leading to a significant savings in execution time without affecting the total flux. These numbers are from runs at 1500 \AA with the dust distributed as in Model 2; similar results are obtained at 2300 \AA and for Model 1.

It is tempting to assume that single scattering provides a reasonable estimate of the diffuse flux, especially in regions of low optical depth ([Murthy & Henry 1995](#); [Henry et al. 2015](#)) because the solution may be derived exactly without recourse to Monte Carlo methods. I have plotted the ratio between the two for $a = 0.4$ and $g = 0.3$ in Fig. 4. Even at the lowest reddening, multiple scattering gives about 25% more flux rising to about 40% more by $E(B - V) = 1.5$, although the exact value will depend on the local geometry between the stars and the dust. Much of this excess is simply because the photon still carries energy after the first interaction which is disregarded in the single scattering assumption.

I have added the flux over the entire model sky for each combination of the optical constants in Fig. 5 and 6. Unlike

³ <http://hpux.connect.org.uk/hppd/hpux/Maths/Misc/randlib-1.3/readme.html>

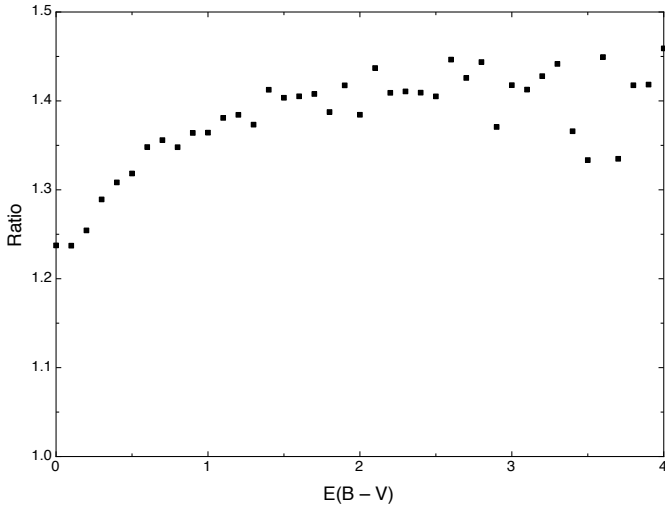


Figure 4. Ratio between multiple and single scattering as a function of $E(B - V)$ with $a = 0.4$ and $g = 0.3$.

Table 1. Five Brightest Stars

Star Name	HIP No.	Percentage of Total
Model 1		
β Cen	68702	3.5
ζ Ori	26727	3.1
ϵ Ori	26311	2.8
α Cru	60718	2.7
ζ Pup	39429	2.0
Model 2		
α Cru	60718	5.6
β Cru	62434	4.2
ζ Ori	26727	2.7
ζ Oph	81377	2.6
ϵ Ori	26311	2.3

the single scattering case where the total flux should rise linearly with the albedo, the total flux rises as approximately the square of the albedo when multiple scattering is taken into account. The flux decreases with increasing g as the photon is more likely to stay within the Galaxy for isotropic scattering and there are more scatterings per photon.

The above results depend little on the distribution of the dust. On the other hand the distance of the scattering locations from the Sun does depend on the dust distribution but not on the optical parameters. I have plotted the percentage of flux originating in 10 pc bins as a function of distance from the Sun in Fig. 7. About half of the observed radiation originates within 100 - 200 pc from the Sun and none from cells more than 600 pc away. The average distance between scatters is also dependent on the dust distribution (Fig. 8). About 60% of the photons are scattered within 200 pc of their origin in Model 1 and more than 90% in Model 2. Virtually all the photons travel less than 500 pc before being scattered. The optical depth per bin is higher in Model 2 (Fig. 2) and most photons will not travel more than one optical depth before interacting with a dust grain.

The diffuse flux from our Galaxy is dominated by a handful of stars (Table 1) with 23% and 27% of the total flux

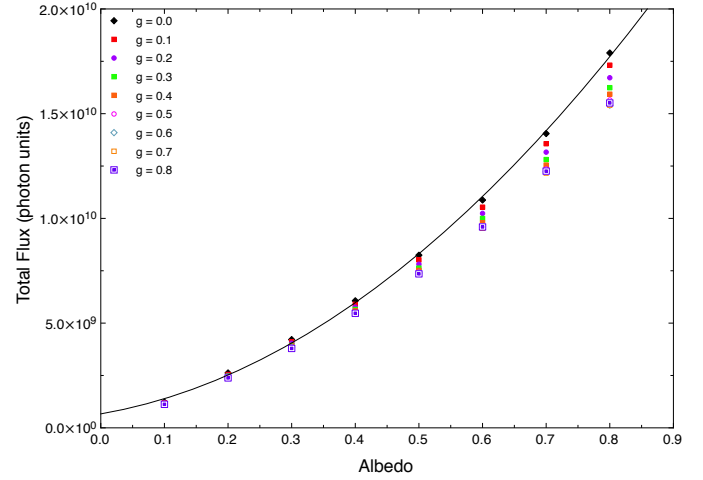


Figure 5. The total flux over the entire sky is shown as a function of albedo for a range of g . The line represents a quadratic fit to the $g = 0$ points and is shown for comparison only.

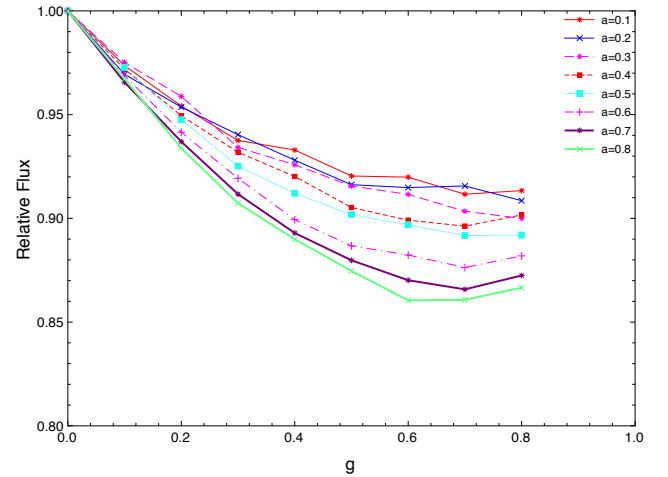


Figure 6. The flux over the entire sky is shown as a function of g for different values of the albedo (see legend). The fluxes for each albedo have been divided by the flux at $g = 0$.

coming from only 10 stars for Models 1 and 2, respectively, and 90% of the total observed flux (Fig. 9) from the 1000 brightest stars. I have plotted the predictions from Model 2 at 1500 \AA in Fig. 10 for $a = 0.4$ and $g = 0$ (isotropic scattering), $g = 0.5$ and $g = 0.8$. I have superimposed the 1000 brightest stars as circles, each with a radius proportional to the log of the brightness. The three images are superficially similar with Gould's Belt prominent in all three. As would be expected, the diffuse light is more spread out for more isotropic scattering and is concentrated near the stars for strongly forward scattering grains.

5 COMPARISON WITH DATA

The main motivation for this study was the availability of the all-sky *GALEX* data which allows tests of the scattering

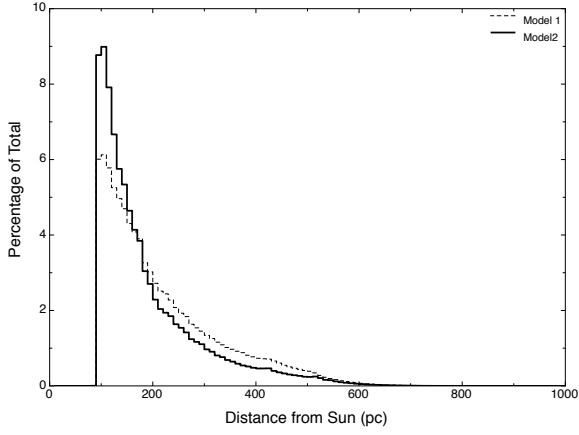


Figure 7. The percentage of the flux in each 10 pc bin is shown as a function of distance from the Sun for $a = 0.4$ and $g = 0$ for the two models. Both models include a cavity of 80 pc radius around the Sun.

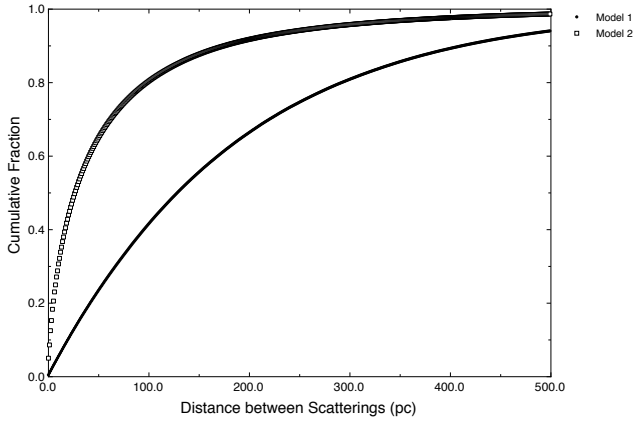


Figure 8. The percentage of the total diffuse flux as a function of distance between scatterings is shown.

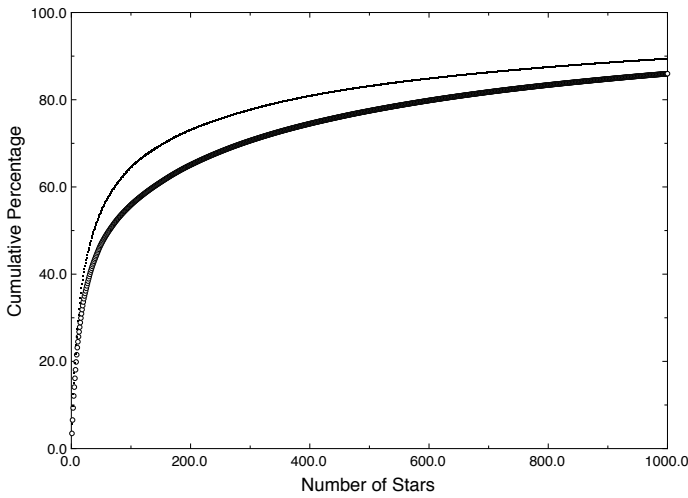


Figure 9. The cumulative contribution of the brightest stars is shown for Models 1 and 2.

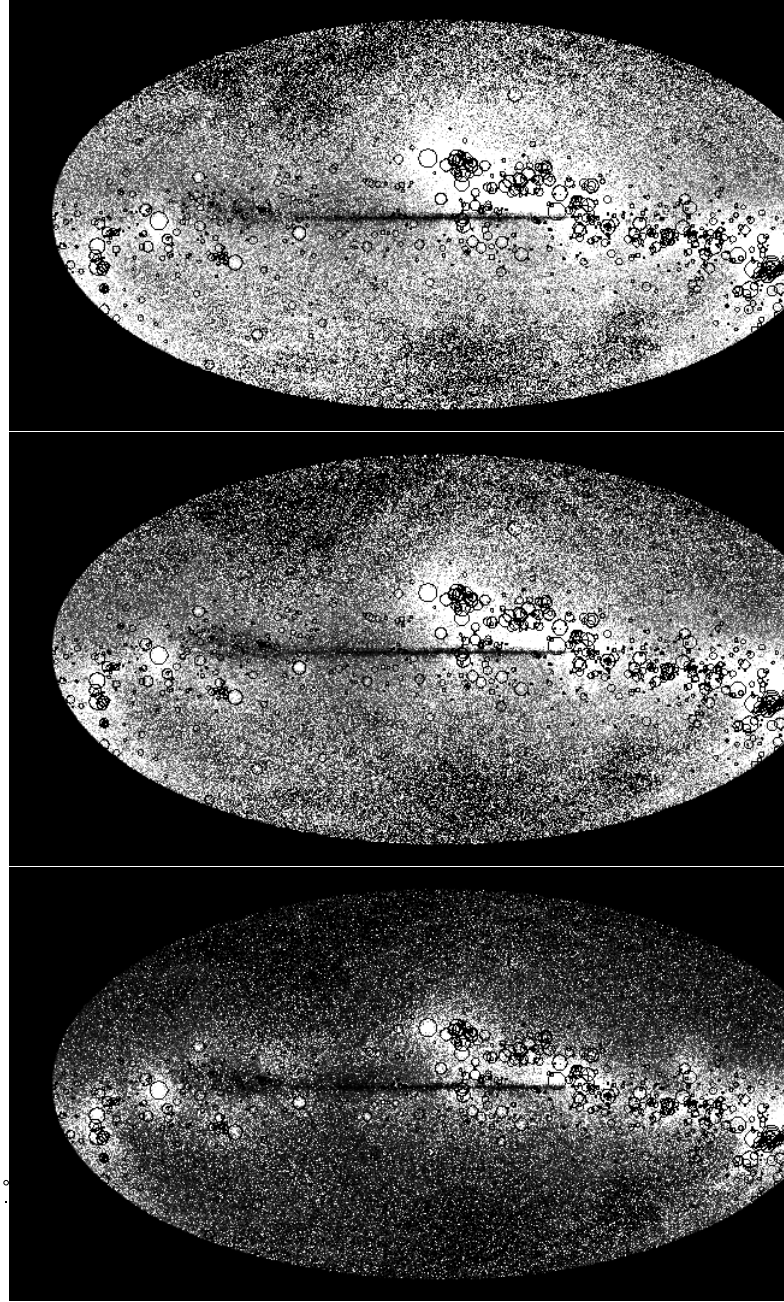


Figure 10. Model 2 predictions at 1500 \AA for $a = 0.4$ and $g = 0$ (top), $g = 0.4$ (middle), and $g = 0.8$ (bottom). The brightest stars are plotted as circles with the radius proportional to the log of the brightness at 1500 \AA . Similar results are obtained at 2300 \AA and for Model 1.

Table 2. Best Fit Parameters

Model	a	g	Slope	y_0	χ^2	r
FUV						
Model 1	0.3	0.1	1.22	-184	3.15	0.861
Model 2	0.4	0.0	0.91	395	3.39	0.875
NUV						
Model 1	0.4	0.0	1.23	-132	4.18	0.863
Model 2	0.5	0.0	0.74	784	5.87	0.771

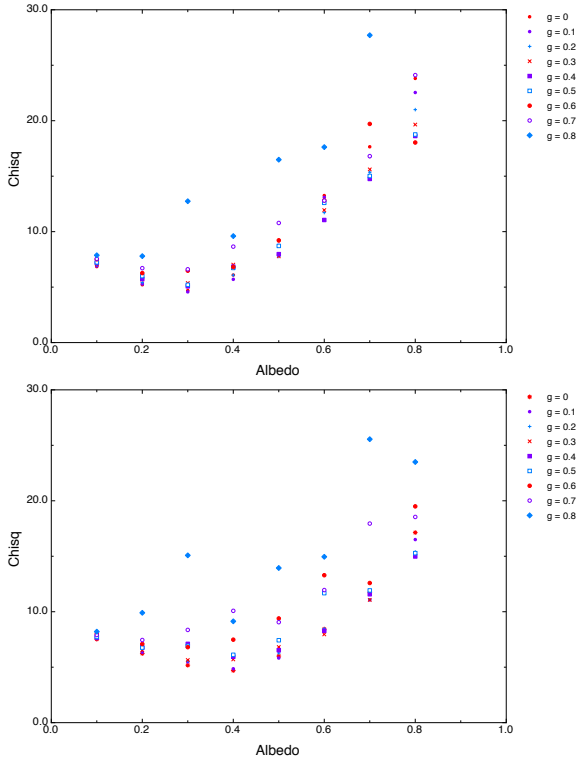


Figure 11. χ^2 plotted as a function of the optical constants for the two models for the FUV band.

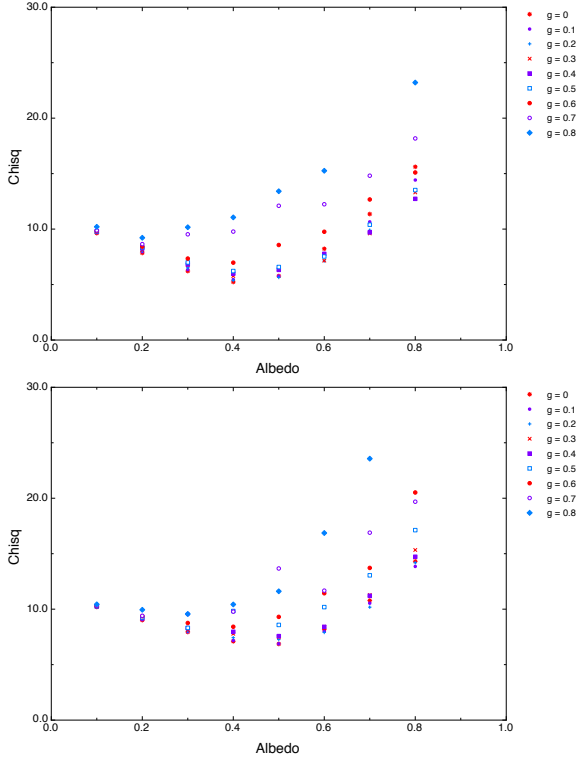


Figure 12. χ^2 plotted as a function of the optical constants for the two models for the NUV band.

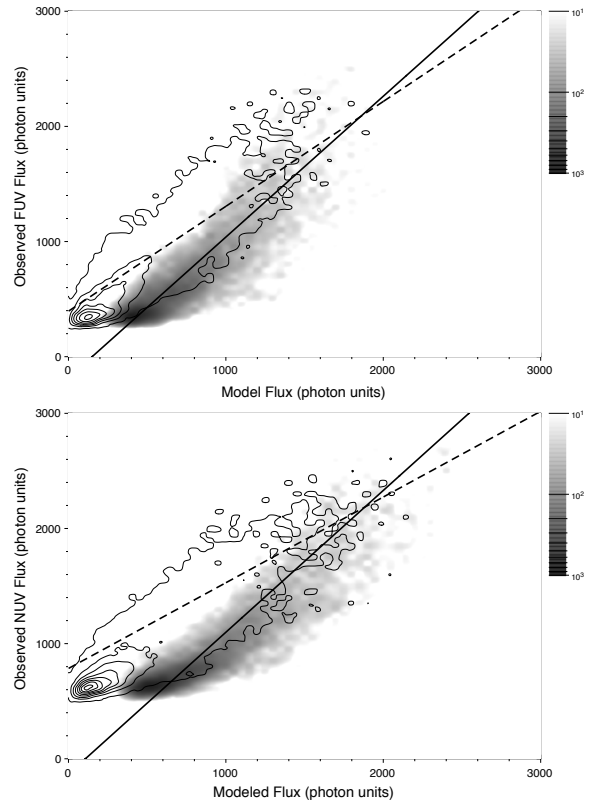


Figure 13. Density plot of the modelled flux versus the observed flux for Model 1 (shading) and Model 2 (contours) for the FUV (left) and NUV (right). The solid line shows the least squares fit to Model 1 and the dashed line shows the least squares fit to Model 2.

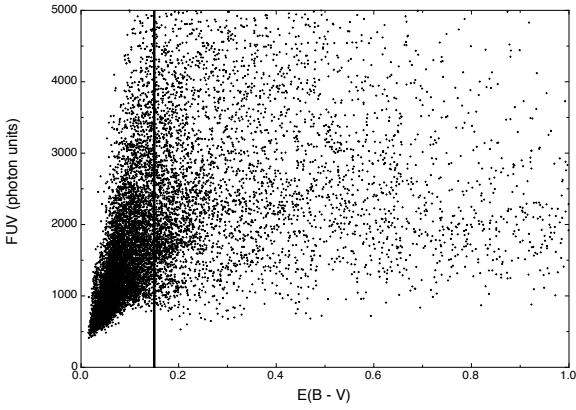
on both small and large scales (Fig. 1). I have tested both Model 1 and Model 2 for a range of optical constants using 50 million input photons and have plotted the reduced χ^2 of the fit between each of the models and the data for the FUV channel in Fig. 11 and for the NUV in Fig. 12. In each case the best fit value of the albedo is between 0.3 and 0.5 and g is close to 0. I then ran the model for each of the dust distributions with a larger number of photons ($> 10^9$) for the best fit case to reduce the noise in the simulations. I have plotted the correlations between the observed and the model fluxes in Fig. 13 with the parameters for the best linear fit between the model and the data listed in Table 2.

The predictions of both models for the dust distribution are generally consistent with the data suggesting that, at least on a global scale, an accurate knowledge of the dust distribution may not be critical in determining the diffuse background. Rather, much of the structure seen in the diffuse background is due to the stellar distribution. This is even more apparent at still shorter wavelengths (Murthy & Sahnow 2004) where there are many fewer bright stars. I will look more closely at the distribution of the background in different sections of the Galaxy in the following paragraphs (Table 3). I will focus only on Model 2, where the dust distribution is more closely reproduced.

The range of $E(B - V)$ is greatest at low latitudes with the expected areas of high extinction near the plane but with surprisingly low values even short distances away from the plane. I have plotted the observed FUV as a function of $E(B$

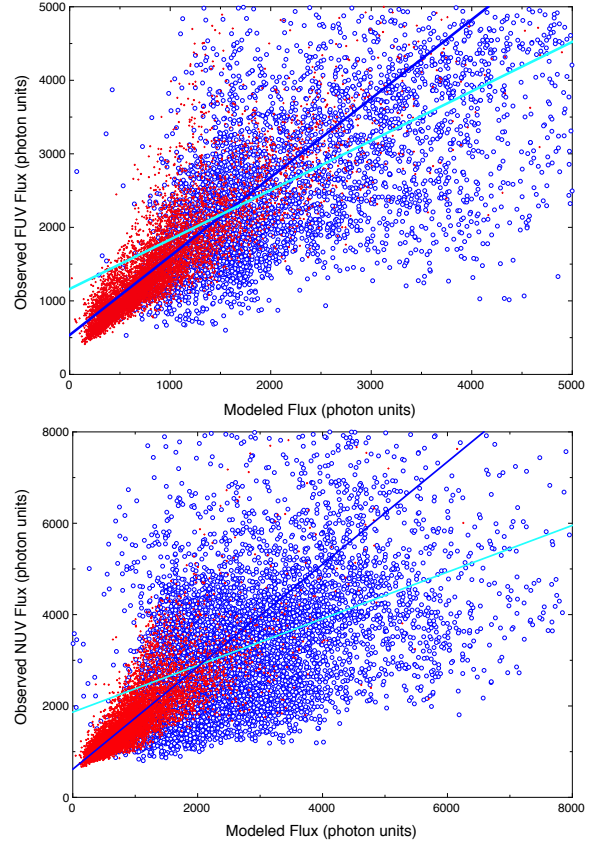
Table 3. Latitudinal Fits

Range	a	g	Slope	y_0	χ^2	r
FUV						
$ b < 30; \tau < 1$	0.4	0.0	1.07	535	8.65	0.850
$ b < 30; \tau > 1$	0.4	0.0	0.67	1163	16.38	0.715
$30 < b < 60$	0.4	0.0	0.96	299	4.01	0.916
$-60 < b < -30$	0.4	0.0	0.64	403	4.27	0.848
$60 < b $	0.4	0.0	0.34	334	4.36	0.426
$-60 > b $	0.4	0.0	0.35	314	3.41	0.579
NUV						
$ b < 30; \tau < 1$	0.5	0.0	1.12	613	10.2	0.810
$ b < 30; \tau > 1$	0.5	0.0	0.51	1869	21.89	0.579
$30 < b < 60$	0.5	0.0	0.68	575	5.52	0.877
$-60 < b < -30$	0.5	0.0	0.56	660	7.48	0.569
$60 < b $	0.5	0.0	0.29	596	8.90	0.395
$-60 > b $	0.5	0.0	0.17	634	8.62	0.277


Figure 14. Observed FUV flux plotted versus $E(B - V)$ for $|b| < 30^\circ$. The solid line represents an $E(B - V)$ of 0.15 which corresponds to an optical depth of 1 in both the FUV and NUV *GALEX* bands. The NUV plot is similar and I have not shown it.

$-V$) in Fig. 14 and divided the observations into two regions: $E(B - V) < 0.15$ and $E(B - V) > 0.15$, approximately corresponding to an optical depth of 1 in both *GALEX* bands. There is an excellent correlation between the model and the data at low optical depths in both bands (Fig. 15) but with an offset of $500 - 600 \text{ ph cm}^{-2} \text{ s}^{-1} \text{ sr}^{-1} \text{ \AA}^{-1}$. There is considerably more scatter between the model and the observations at greater optical depths where the structure of the dust is likely to be more complex and local effects may determine the observed background. One example of this was seen in the vicinity of the Coalsack Nebula where [Murthy et al. \(1994\)](#) found that the intense diffuse emission was due to the scattering of the light of only three bright stars by a thin layer of dust in front of the dense molecular cloud.

The range of $E(B - V)$ is much less at mid-latitudes ($30 < |b| < 60$) and there is a good correlation between the modelled and the observed fluxes in both the FUV and the NUV (Table 3) with an offset of $500 - 600 \text{ ph cm}^{-2} \text{ s}^{-1} \text{ sr}^{-1} \text{ \AA}^{-1}$, just as at lower latitudes. However, the fit is much better in the Northern hemisphere for both the FUV and the NUV bands (Fig. 16), reflecting the smaller scatter in the ratio of the UV flux to the reddening in the Northern hemisphere (Fig. 17). In addition, individual bright spots around hot stars (seen clearly in the NUV image of Fig. 1)


Figure 15. Observed flux at low Galactic latitudes plotted versus predicted flux for $\tau < 1$ (red) and $\tau > 1$ (blue) for FUV (top) and NUV (bottom) bands.

are due to dust near to the star which may not be reproduced by a generic dust distribution.

The dust scattered light at high latitudes is due to the back scattering of light from Galactic plane stars ([Jura 1979](#)) and would be expected to be proportional to the reddening. However, this is not seen in the data (Fig. 18) and, as a result, the models naturally do not fit the data well (Fig. 19). There is an offset of about $300 \text{ ph cm}^{-2} \text{ s}^{-1} \text{ sr}^{-1} \text{ \AA}^{-1}$ and $600 \text{ ph cm}^{-2} \text{ s}^{-1} \text{ sr}^{-1} \text{ \AA}^{-1}$ between the model predictions and the data in the FUV and the NUV, respectively, at both the North and the South poles, consistent with most high latitude observations ([Anderson et al. 1979](#); [Paresce et al. 1979, 1980](#); [Zvereva et al. 1982](#); [Joubert et al. 1983](#); [Jakobsen et al. 1984](#); [Tennyson et al. 1988](#); [Onaka et al. 1989](#)). It was recognized that this was too high to be explained by dust scattering and was generally thought to be due to an extragalactic background (see [Bowyer \(1991\)](#); [Henry \(1991\)](#) for discussion and references). However, [Henry \(2010\)](#) pointed out that UV observations of the high latitude Sandage clouds ([Sujatha et al. 2009](#)) show no evidence of the clouds, neither in scattered light nor as a shadow against an extragalactic background, thereby indicating an unknown origin.

In addition, the slope of ≈ 0.3 in both bands between the model and the observed data suggests that only about 30% of the flux is due to dust scattered light. It is premature to speculate on why this is so with possible explanations being that the dust-to-gas ratio is different at high latitudes or that the optical properties of the dust are different. There

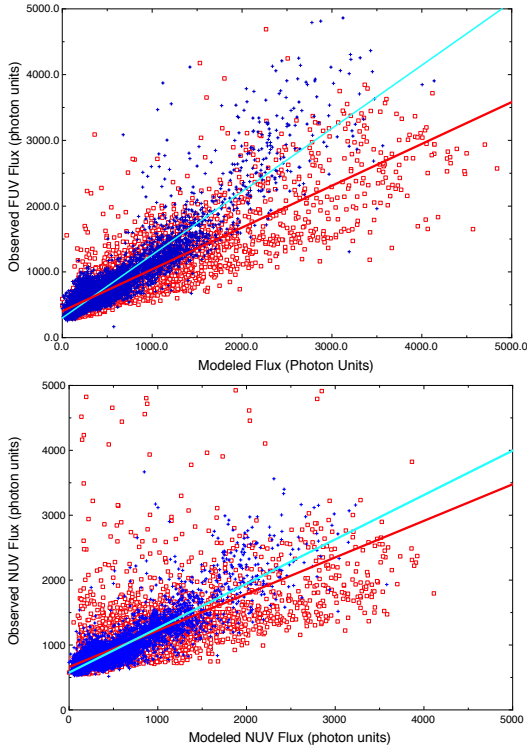


Figure 16. Observed flux at mid-latitudes plotted versus predicted flux for FUV (top) and NUV (bottom). The Northern hemisphere points are plotted in blue and the Southern hemisphere in red. The blue and red lines represent linear fits to both hemispheres.

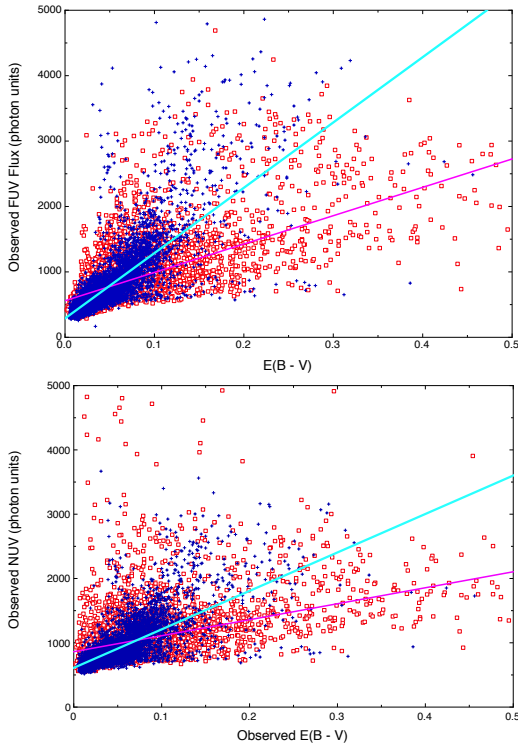


Figure 17. Observed flux at mid-latitudes plotted versus reddening for FUV (top) and NUV (bottom). Colors and lines are as in Fig. 16.

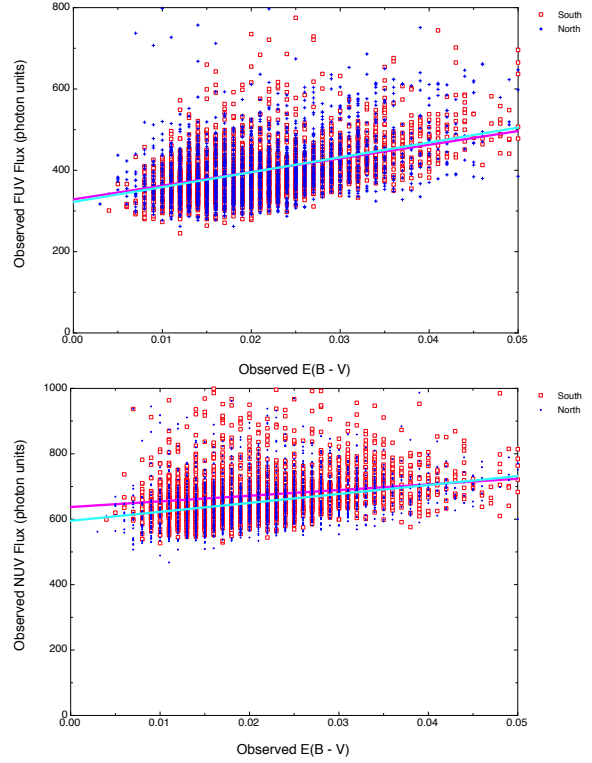


Figure 18. Observed flux at high latitudes plotted versus the reddening.

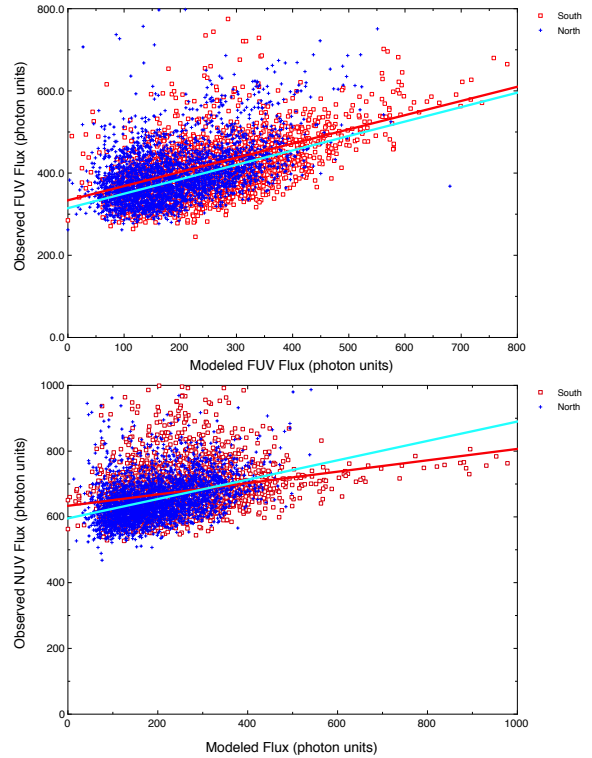


Figure 19. Observed flux at high latitudes plotted versus predicted flux.

are other hidden assumptions in the conversion from E(B - V) as derived from IR observations by Schlegel et al. (1998) to the cross-section in the UV needed for my calculations. There are known to be problems with the reddening derived by Schlegel et al. (1998) in different parts of the Galaxy (eg., Peek & Graves (2010)) and these uncertainties will have a proportionately greater effect at the small column densities at high latitudes. I will defer this to a future work.

6 SUMMARY

I have presented a Monte Carlo model for calculating the dust scattered starlight over the entire Galaxy. The main conclusions are as follows:

(i) A multiple scattering model increases the scattered flux by about 30% over the single scattering approximation regardless of the optical depth.

(ii) The total scattered flux is proportional to the square of the albedo and is greatest for isotropically scattering grains.

(iii) 90% of the diffuse flux originates from less than 1000 stars and 25% from only 10 stars.

(iv) About half of the diffuse radiation seen at the Earth is scattered within 200 pc of the Sun with no radiation arising from further than 600 pc away.

(v) The all-sky diffuse radiation is fit well with $a = 0.4$ and $g = 0$. The albedo is constrained by the total flux while g is constrained by the amount of scattering far from bright stars.

(vi) The model predictions are close to the observed values at low and mid-latitudes for low optical depths but with an offset of $500 - 600 \text{ ph cm}^{-2} \text{ s}^{-1} \text{ sr}^{-1} \text{ \AA}^{-1}$, similar to the offsets seen by Hamden et al. (2013) and Henry et al. (2015). The fit is poorer at larger optical depths where the geometry is more complex.

(vii) Although the optical depth is low at high latitudes, the model does not do a good job of predicting the observed background. The slope between the observed and the modelled flux is only about 0.3 which could be due to many factors from a lower albedo at high latitudes to a different conversion from the infrared emission to the cross-section in the UV.

(viii) There is an offset of $300 \text{ ph cm}^{-2} \text{ s}^{-1} \text{ sr}^{-1} \text{ \AA}^{-1}$ in the FUV band and $600 \text{ ph cm}^{-2} \text{ s}^{-1} \text{ sr}^{-1} \text{ \AA}^{-1}$ in the NUV which is consistent with previous observations and cannot be due to dust scattered radiation.

(ix) The software has been released under a non-restrictive license.

7 FURTHER WORK

The local geometry of the exciting stars and the scattering dust are important in determining the diffuse background over much of the sky and their effects can be seen in Fig. 1 where there are extended halos around bright stars such as Spica. There have been important new studies of the 3-dimensional distribution of the dust, most recently by Green et al. (2015), which I will implement. It is likely that, at least in some parts of the sky, observations of the scattering will be better able to constrain the distance and density of the

dust clouds than the standard extinction methods (Lee et al. 2006).

One of the major constraints in this work is the noise intrinsic to Monte Carlo modelling which can only be reduced by increasing the number of photons. Fortunately, Monte Carlo lend themselves well to modern HPC (high-performance computing) methods as well as processing on the GPU (graphics processing unit) and the next step is to port the software to that environment.

ACKNOWLEDGEMENTS

This research has made use of NASA's Astrophysics Data System Bibliographic Services. I have used the GnuDataLanguage (<http://gnudatalanguage.sourceforge.net/index.php>) for the analysis of this data. The data presented in this paper were obtained from the Mikulski Archive for Space Telescopes (MAST). STScI is operated by the Association of Universities for Research in Astronomy, Inc., under NASA contract NAS5-26555. Support for MAST for non-HST data is provided by the NASA Office of Space Science via grant NNX09AF08G and by other grants and contracts.

REFERENCES

- Anderson, R. C., Henry, R. C., Brune, W. H., Feldman, P. D., & Fastie, W. G. 1979, *ApJ*, 234, 415
- Bowyer, S. 1991, *ARA&A*, 29, 59
- Castelli, F., & Kurucz, R. L. 2004, *arXiv:astro-ph/0405087*
- Draine, B. T. 2003, *ARA&A*, 41, 241
- Edelstein, J., Min, K.-W., Han, W., et al. 2006, *ApJ*, 644, L153
- Gordon, K. D., Misselt, K. A., Witt, A. N., & Clayton, G. C. 2001, *ApJ*, 551, 269
- Green, G. M., Schlafly, E. F., Finkbeiner, D. P., et al. 2015, *ApJ*, 810, 25
- Hamden, E. T., Schiminovich, D., & Seibert, M. 2013, *ApJ*, 779, 180
- Hayakawa, S., Yamashita, K., & Yoshioka, S. 1969, *Ap&SS*, 5, 493
- Henry, R. C. 1977, *ApJS*, 33, 451
- Henry, R. C. 1991, *ARA&A*, 29, 89
- Henry, R. C. 2010, *Mem. Soc. Astron. Italiana*, 81, 63
- Henry, R. C., Murthy, J., Overduin, J., & Tyler, J. 2015, *ApJ*, 798, 14
- Henry, L. G., & Greenstein, J. L. 1941, *ApJ*, 93, 70
- Jakobsen, P., Bowyer, S., Kimble, R., et al. 1984, *A&A*, 139, 481
- Joubert, M., Deharveng, J. M., Cruvellier, P., Masnou, J. L., & Lequeux, J. 1983, *A&A*, 128, 114
- Jura, M. 1979, *ApJ*, 227, 798
- Lee, D.-H., Yuk, I.-S., Jin, H., et al. 2006, *ApJ*, 644, L181
- Marshall, D. J., Robin, A. C., Reylé, C., Schultheis, M., & Picaud, S. 2006, *A&A*, 453, 635
- Martin, D. C., Fanson, J., Schiminovich, D., et al. 2005, *ApJ*, 619, L1
- Morrissey, P., Conrow, T., Barlow, T. A., et al. 2007 *ApJS*173, 682
- Murthy, J. 2009, *Ap&SS*, 320, 21
- Murthy, J. 2014b, *ApJS*, 213, 32
- Murthy, J., & Henry, R. C. 1995, *ApJ*, 448, 848
- Murthy, J., & Henry, R. C. 2011, *ApJ*, 734, 13
- Murthy, J., & Sahnou, D. J. 2004, *ApJ*, 615, 315
- Murthy, J., Henry, R. C., & Holberg, J. B. 1994, *ApJ*, 428, 233
- Onaka, T., Tanaka, W., Watanabe, T., et al. 1989, *ApJ*, 342, 238

- Paresce, F., Bowyer, S., Lampton, M., & Margon, B. 1979, *ApJ*, 230, 304
- Paresce, F., McKee, C. F., & Bowyer, S. 1980, *ApJ*, 240, 387
- Peek, J. E. G., & Graves, G. J. 2010, *ApJ*, 719, 415
- Perryman, M. A. C., Lindegren, L., Kovalevsky, J., et al. 1997, *A&A*, 323, L49
- Schiminovich, D., Friedman, P. G., Martin, C., & Morrissey, P. F. 2001, *ApJ*, 563, L161
- Schlegel, D. J., Finkbeiner, D. P., & Davis, M. 1998, *ApJ*, 500, 525
- Seon, K.-I. 2015, *Journal of Korean Astronomical Society*, 48, 57
- Steinacker, J., Baes, M., & Gordon, K. D. 2013, *ARA&A*, 51, 63
- Sujatha, N. V., Murthy, J., Karnataki, A., Henry, R. C., & Bianchi, L. 2009, *ApJ*, 692, 1333
- Tennyson, P. D., Henry, R. C., Feldman, P. D., & Hartig, G. F. 1988, *ApJ*, 330, 435
- Welsh, B. Y., Lallement, R., Vergely, J.-L., & Raimond, S. 2010, *A&A*, 510, A54
- Yusef-Zadeh, F., Morris, M., & White, R. L. 1984, *ApJ*, 278, 186
- Zvereva, A. M., Severnyi, A. B., Granitskii, L. V., et al. 1982, *A&A*, 116, 312

This paper has been typeset from a $\text{\TeX}/\text{\LaTeX}$ file prepared by the author.